

**NONLINEAR FINITE ELEMENT MODELLING AND PARAMETRIC STUDY OF
CFRP SHEAR-STRENGTHENED PRESTRESSED CONCRETE GIRDERS**

Michael Qapo (Corresponding author)

PhD Candidate

mkq118@bham.ac.uk

Phone number: +44 7407 268616

School of Civil Engineering, University of Birmingham, Edgbaston, Birmingham, B15 2TT,
United Kingdom

Samir Dirar

Lecturer in Structural Engineering

s.m.o.h.dirar@bham.ac.uk

School of Civil Engineering, University of Birmingham, Edgbaston, Birmingham, B15 2TT,
United Kingdom

Jian Yang

Lecturer in Structural Engineering

j.yang.3@bham.ac.uk

School of Civil Engineering, University of Birmingham, Edgbaston, Birmingham, B15 2TT,
United Kingdom

Mohammed Z. E. B. Elshafie

Lecturer in Construction Engineering

me254@cam.ac.uk

Department of Engineering, University of Cambridge, Trumpington Street, Cambridge,
CB2 1PZ, United Kingdom

Abstract:

This paper presents a three-dimensional nonlinear finite element (FE) model for prestressed concrete girders strengthened in shear with externally bonded carbon fibre reinforced polymer (CFRP) reinforcement. A total strain rotating crack model, where the crack direction changes with the change in the direction of the principal tensile stress, was used for the concrete. In this model, explicit modelling of the concrete shear behaviour after cracking, e.g. via a shear retention parameter, is not required as the crack plane is always a principal plane with no shear stresses. The FE model was validated using experimental results from the literature. An extensive parametric study was carried out to identify the effect of the concrete compressive strength, CFRP width-to-spacing ratio, CFRP thickness, girder effective depth, shear span to effective depth ratio, level of prestress, tendon profile, pre-cracking and CFRP-to-concrete interface model on the predicted shear force capacity. The results suggested that the predicted shear strength enhancement can be significant and increases with the increase in concrete compressive strength, CFRP width-to-spacing ratio, and CFRP thickness but decreases with the increase in girder effective depth and shear span to effective depth ratio.

Keywords: fibre reinforced polymer; finite element; girder; prestressed concrete; shear; strengthening

Highlights:

- A FE model for shear-strengthened prestressed concrete girders was developed.
- The FE model was validated using experimental results from the literature.
- The influence of the factors affecting the predicted shear strength was identified.
- The predicted shear strength enhancement can be significant.

1 Introduction

The shear strength deficiency of existing prestressed concrete (PC) bridges is a global issue faced by the owners and managers of transport infrastructures (Middleton 1997; Nanni et al. 2004; Valerio et al. 2009). The underlying causes of this issue include heavier traffic loads, corrosion of the internal steel reinforcement, structural deterioration due to ageing, poor initial design, more stringent assessment codes, aggressive exposure conditions, and natural or manmade extreme events (Valerio et al. 2009; Petty et al. 2011; Dirar et al. 2013a).

One viable solution is to use externally bonded (EB) carbon fibre reinforced polymer (CFRP) reinforcement as shear strengthening systems for existing PC bridges. EB CFRP shear strengthening systems have several advantages over traditional strengthening systems, such as high strength to weight ratio, ease of use, and resistance to corrosion (ACI 440R-07 2007; Murphy et al. 2012). In recent years, the successful use of the EB CFRP shear strengthening technique for PC girders has been demonstrated (Petty et al. 2011; Murphy et al. 2012; Kang and Ary 2012). However, a careful review of the published literature reveals that the majority of the research work has been experimental and focused on verifying the effectiveness of the technique. Although physical testing provides valuable information on the overall performance of girders and the local behaviour of constituent materials, high costs associated with the production of large-scale specimens often restricts the evaluation of the parameters influencing the shear behaviour of the strengthened girders (You et al. 2011).

The Finite Element Method (FEM) provides a cost-effective tool for carrying out extensive parametric studies on CFRP shear-strengthened PC girders. The FEM can be used to model various combinations of geometric and loading conditions. The nonlinear behaviour of CFRP shear-strengthened PC girders can be taken into consideration by incorporating appropriate constitutive laws and iterative procedures (You et al. 2011). Nonetheless, numerical

research studies on CFRP shear-strengthened PC girders (Petty et al. 2011; You et al. 2011) are scarce. Moreover, to date, extensive studies examining the influencing parameters of the behaviour of CFRP shear-strengthened PC girders have not been found. This was partially attributed to the complex behaviour of CFRP shear-strengthened PC girders (You et al. 2011).

This paper presents a three-dimensional nonlinear finite element (FE) model for CFRP shear-strengthened PC girders using the commercial FE package DIANA Version 9.4.4 (DIANA User's Manual 2012). The FE model is validated by using experimental results from the published literature (Kang and Ary 2012). The validated FE model is then used to examine the effect of the concrete compressive strength, CFRP width-to-spacing ratio, CFRP thickness, girder effective depth, shear span to effective depth ratio, level of prestress, tendon profile, pre-cracking, and CFRP-to-concrete interface model on the predicted strength of PC girders strengthened in shear with EB CFRP reinforcement.

2 Summary of the experimental work

The FE model reported in this paper was validated using the experimental work carried out by Kang and Ary (2012). They tested three I-shaped PC girders in a four-point-bending configuration. One girder was used as a control specimen whereas the remaining two girders (IB-05 and IB-10) were strengthened with U-shaped EB multi-directional CFRP strips before testing. The three girders had a shear span to effective depth ratio (a/d) of 2.5 and were designed to fail in shear.

The unstrengthened cross-section of the tested girders is shown in Fig. 1. Each girder had two $\text{Ø}12$ mm steel bars in the compression flange. The tension flange reinforcement included two $\text{Ø}25$ mm bars, two $\text{Ø}20$ mm bars, and two $\text{Ø}12.5$ mm tendons prestressed to 1075 MPa. Single-leg $\text{Ø}10$ mm steel bars were used as stirrups within the constant moment zone whereas no internal shear reinforcement was used within the shear spans. In practice,

however, prestressed concrete girders usually include at least a minimum amount of internal steel shear reinforcement. Kang and Ary (2012) reported that they excluded steel shear reinforcement from the shear spans because their experimental programme was designed to study the bond behaviour between EB CFRP shear reinforcement and concrete in the absence of internal steel shear reinforcement.

The external shear reinforcement consisted of one layer of 76 mm wide × 1.25 mm thick EB CFRP strips. Strip spacing was the only studied parameter in the experimental programme. The centre-to-centre spacing between the EB CFRP strips was 127 mm in the case of IB-05 and 254 mm in the case of IB-10 as shown in Fig. 2.

Table 1 summarises the mechanical properties of the concrete, steel reinforcement bars, seven-wire strands (tendons), and EB CFRP strips used in the experimental investigation.

3 Finite element model

In order to properly model the bond-slip behaviour at the CFRP-to-concrete interface, a three-dimensional FE model incorporating interface elements was developed. The constitutive models and element types were carefully selected to model the experimental behaviour of the tested girders. The double symmetry of the tested girders about both the mid-span and mid-width planes enabled a quarter-model to be developed as depicted in Fig. 3. Appropriate boundary conditions were applied by restraining the movement of the planes of symmetry at mid-span and mid-width in the X and Z directions (see Fig. 3) respectively and allowing movement in the vertical (Y) direction.

The following subsections describe briefly the element types and constitutive models used in the FE model. Further information can be found in DIANA User's Manual (2012).

3.1 Concrete

The concrete was modelled using eight-node isoparametric solid brick elements that have three translational degrees of freedom at each node. The stress field in these elements is three-dimensional, and both the loading and principal stress can be in any direction. Several concrete element sizes were investigated. An average element size of $3d_a$ (30 mm) gave the best predictions as demonstrated in Section 4 (d_a is the maximum aggregate size). This is consistent with the recommendation of Bažant and Oh (1983) to use an element size of three times the maximum aggregate size.

A total strain rotating crack model based on the smeared crack concept was used for the concrete. In this model, the crack direction changes with the change in the direction of the principal tensile stress. Hence, the crack plane is always a principal plane with no shear stresses. Therefore, explicit modelling of the concrete shear behaviour after cracking, e.g. via a shear retention parameter, is not required.

The behaviour of concrete in compression and tension was modelled with a uniaxial stress-strain relationship which is evaluated in the principal direction of strains. A Poisson's ratio of 0.15 gave the best predictions as demonstrated in Section 4. This is consistent with the recommendation of CEB-FIP Model Code 1990 (1993).

The concrete in compression was modelled by Thorenfeldt et al.'s (1987) stress-strain curve which is given by:

$$\frac{f_c}{f'_c} = \frac{n \left(\frac{\varepsilon_c}{\varepsilon_{co}} \right)}{n - \left(1 - \left(\frac{\varepsilon_c}{\varepsilon_{co}} \right)^{nk} \right)} \quad (1)$$

where f'_c is the concrete compressive strength, ε_{co} is the strain corresponding to the concrete compressive strength (automatically calculated by the FE package), $n = 0.18 + (f'_c/17)$, and k is a parameter controlling the post-peak branch of the stress-strain curve. The only parameter required by the FE package to define the stress-strain curve is the concrete

compressive strength. The softening of concrete in compression due to lateral tensile strain was considered by incorporating the model proposed by Vecchio and Collins (1993).

For concrete in tension, a multi-linear quasi-brittle model was used. This model consisted of a linear tensile stress-tensile strain relationship up to the value of the concrete tensile strength with a slope equal to the concrete elastic modulus. The post-peak behaviour was represented by a drop in the tensile stress to a value just higher than zero so as to ensure analysis stability. The use of this quasi-brittle model may be justified by the fact that internal reinforcement was not used in the shear spans of the girders.

3.2 Steel plates

Three steel plates were used in the FE model, namely loading, support and end plates. The loading and support plates were modelled by solid six-node isoparametric wedge elements, whereas solid eight-node isoparametric brick elements were used to model the end plate. The end plate was used to avoid stress concentrations in the concrete elements. Such stress concentrations are caused by the prestressing force and may lead to convergence difficulties.

The behaviour of the three steel plates in both compression and tension was modelled by an elastic-perfectly plastic model with von-Mises yield criterion (DIANA User's Manual 2012).

3.3 Steel reinforcement and tendons

Both the steel reinforcement and tendons were represented by embedded bar elements. The embedded bar elements are truss-like elements with no degrees of freedom of their own and their strains are calculated from the displacement field of the surrounding concrete elements (DIANA User's Manual 2012). Bond failure was not the governing failure mode hence perfect bond was assumed between the embedded bar elements and the concrete elements.

An elastic-perfectly plastic model was used for both the longitudinal steel reinforcement and the stirrups. The experimentally measured yield strength values, as reported in Table 1, were used.

For the prestressing tendons, an elastic-plastic model combined with von-Mises yield criterion (DIANA User's Manual 2012) was employed. The experimental stress-strain relationship depicted in Fig. 4 was considered.

3.4 CFRP strips

The CFRP strips were modelled as an isotropic material because multi-directional fibres were used in the experimental work. Geometrical modelling comprised four-node quadrilateral isoparametric curved shell elements which are a combination of plate bending and plane stress elements (DIANA User's Manual 2012). Material modelling consisted of a linear stress-strain relationship up to the ultimate tensile strength of the CFRP strips (see Table 1).

3.5 CFRP-to-concrete interface

The bond zone between the concrete and EB CFRP strips was simulated using eight-node plane quadrilateral interface elements. These elements are used to connect two planes in three-dimensional models. For further details, see DIANA Element Library (DIANA User's Manual 2012).

In this study, the bi-linear bond-slip model developed by Sato and Vecchio (2003) was adopted for modelling the CFRP-to-concrete interface. This model assumes that bond failure occurs within a thin layer of concrete adjacent to the concrete-to-adhesive interface because the adhesive is usually stronger than the concrete. Hence, the bond-slip model simulates the overall behaviour of the CFRP-to-concrete interface rather than the adhesive material.

The adopted bi-linear bond-slip model is shown in Fig. 5 and given by:

$$\tau_{max} = (54f'_c)^{0.19} \quad (2)$$

$$S_0 = 0.057 \sqrt{G_{f,i}} \quad (3)$$

$$S_u = \frac{2G_{f,i}}{\tau_{max}} \quad (4)$$

$$G_{f,i} = \left(\frac{\tau_{max}}{6.6} \right)^2 \quad (5)$$

where τ_{max} is the peak bond stress, S_0 is the slip corresponding to the peak bond stress, S_u is the ultimate slip, and $G_{f,i}$ is the interfacial fracture energy. Debonding starts when the slip value exceeds S_0 . Complete debonding occurs when the slip value reaches S_u .

3.6 Solution procedure

DIANA Phased Analysis Module (DIANA User's Manual 2012) was used to model the different construction and loading stages of the tested girders. A phased analysis consists of several calculation phases. The FE model may be modified amongst phases by the addition or removal of elements or boundary conditions. In nonlinear phased analysis, the results of the last step in a given phase are used as initial values for the first step in the following phase (Dirar et al. 2013b).

Except for the pre-cracked FE models described in Section 5.8, two nonlinear calculation phases were used throughout this study. In Phase I, the elements representing the EB CFRP reinforcement and the FRP-to-concrete interface were set as inactive and the unstrengthened FE model was prestressed. Phase II included activating the elements representing the EB CFRP reinforcement and the FRP-to-concrete interface, and then loading the FE model up to failure. This technique accurately modelled the physical tests.

An incremental-iterative procedure was employed to achieve convergence. Loads were applied using vertical displacement increments of 0.1 mm. The quasi-Newton iteration method (or Secant method) was used, together with a displacement-based convergence

criterion, to achieve equilibrium at the end of each increment. Based on Hee and Jefferson (2008), a displacement norm value of 0.001 was used to specify convergence. This strategy proved to be successful as convergence was achieved at every load increment.

4 Validation of the FE model

The experimental work described in Section 2 was used to validate the developed FE model. The comparison between the numerical and experimental results included the shear force capacity, shear-force versus mid-span deflection curves and crack patterns at failure. No strain gauges were used to measure the CFRP strain during testing. Therefore, the CFRP strain predictions are not presented herein.

Table 2 gives the experimental (V Exp.) and FE-predicted (V FE) shear forces at failure. The FE model predicted the experimental shear force capacities of the tested PC girders with a mean experimental/predicted ratio of 0.90 and a standard deviation of 0.10. The mid-span deflections at failure of the tested PC girders were predicted with a mean experimental/predicted ratio of 1.06 and a standard deviation of 0.10.

Fig. 6 presents the shear-force versus mid-span deflection results for both the experimental and FE work. It should be noted that Fig. 6 does not show the camber due to prestress. Both the experimental and FE-predicted curves are quasi-linear up to crack formation. After crack formation, both the experimental and numerical curves turned nonlinear due to stiffness deterioration. The post-cracking stiffness, i.e. the slope of the shear force-deflection curve after crack formation, was well modelled. Upon further loading, the post-cracking stiffness continued to deteriorate until failure occurred. At failure, there is a sudden drop in load at peak shear force, which is a characteristic of brittle (shear) failure.

As can be seen from Table 2 and Fig. 6, the FE model with a concrete compressive strength of 59 MPa overestimated the shear force at failure for IB-10. It may be argued that shear failure of concrete beams occurs due to discrete major cracks whereas the FE model is

based on smeared cracking without explicit attention to modelling fast fracture which the mere use of fracture energy on its own, as in the developed FE model, does not capture. However, such an argument is at variance with the experimental/predicted shear force capacity ratios of 0.91 and 1.00 for the control and IB-05 girders respectively (see Table 2). The discrete crack approach, which employs interface elements to introduce a gap in the FE mesh after cracking, is more realistic in modelling shear failure of concrete beams than the smeared crack approach. However, the overall structural behaviour can be well modelled using the smeared crack approach (Sagasetta and Vollum 2009).

A careful analysis of the experimental results (Kang and Ary 2012) shows that IB-10 had a significant lower initial un-cracked stiffness compared to the other two girders (Control and IB-05). Furthermore, the EB CFRP strips used to strengthen IB-10 fractured at failure. Nonetheless, the experimental results suggested that the EB CFRP strips did not enhance the shear force capacity of IB-10 over that of the control girder (see Table 2). These two contradicting results together with the lower un-cracked stiffness for IB-10 may be reconciled by considering a lower compressive strength, and consequently lower initial un-cracked stiffness and unstrengthened shear force capacity, for IB-10. Using a concrete cylinder compressive strength value of 45 MPa gave the best numerical results for IB-10 (see Fig. 6c) in terms of the initial un-cracked stiffness, cracked stiffness, shear force capacity, and mid-span deflection at failure. Further experimental testing for IB-10 with concrete cylinder compressive strengths of 45 MPa and 59 MPa is required in order to confirm the above explanation.

Fig. 7 shows the experimental crack patterns at failure for the three girders together with contour plots of the predicted principal tensile strain in the concrete at the predicted failure loads. It can be seen that the FE model correctly predicted the shear failure mode of the tested girders. The FE model also correctly predicted that the control girder failed due to a major diagonal crack that ran from the support to the loading plate (see Fig. 7a). The

strengthened girders had more distributed diagonal cracks due to the presence of the EB CFRP strips.

5 Parametric study

The following subsections detail the parametric study. A total of 61 nonlinear analyses were carried out to investigate the effect of the parameters influencing the strength of PC girders strengthened in shear with EB CFRP reinforcement. It should be noted that the predicted results reflect the performance of the FE model rather than that of actual girders. Further testing is recommended to confirm the predicted results.

Except for the FE models used to investigate the effect of concrete compressive strength, all the FE models considered in the parametric study had a concrete cylinder compressive strength of 59 MPa. All the modelled girders reported in this study failed in shear. In order to investigate the effect of a given parameter, only its value was varied whereas the values of the other parameters were kept unchanged. For a given FE model, the shear force gain was calculated by subtracting the predicted unstrengthened shear force capacity from the corresponding predicted strengthened shear force capacity.

5.1 Effect of concrete compressive strength

Concrete cylinder compressive strength values of 30 MPa, 40 MPa, 50 MPa, 59 MPa (i.e. similar to the average concrete compressive strength of the tested girders), and 70 MPa were considered for the control as well as the strengthened girders. The FE models used to investigate the effect of concrete compressive strength were nominally identical to those validated in Section 4.

Fig. 8a depicts the influence of concrete compressive strength on the predicted shear force capacity. The FE model predicted that the shear force capacity of the PC girders varies approximately linearly with the cylinder compressive strength. The predicted shear force capacity of the unstrengthened, IB-10, and IB-05 PC girders increased by 62.7%, 61.3%,

and 65.1% respectively when the concrete compressive strength was increased from 30 MPa to 70 MPa. Such significant increases were to be expected because, for PC girders without internal shear reinforcement, the concrete contribution to the shear force capacity is significant. Increasing the concrete compressive strength will therefore increase the concrete contribution and enhance the shear force capacity.

The variation of predicted shear force gain (i.e. predicted CFRP contribution to the shear force capacity) with concrete compressive strength is shown in Fig. 8b. It can be seen that the increase in concrete compressive strength resulted in a corresponding increase in the predicted CFRP contribution especially for the case of IB-05 where a higher CFRP reinforcement ratio was used. The predicted CFRP contributions of IB-10 and IB-05 girders increased from 14.32 KN and 20.64 KN respectively to 21.8 KN and 36.2 KN respectively due to the increase in concrete compressive strength from 30 MPa to 70 MPa. This increase may be attributed to the role of concrete compressive strength in enhancing the bond performance between the EB CFRP reinforcement and the concrete (see Eq. 2). However, the increase in concrete compressive strength did not significantly affect the percentage increase in CFRP contribution; i.e. for a given girder, the CFRP contribution and the concrete contribution increased by approximately equal rates. The average percentage increase in CFRP contribution for IB-10 and IB-05 girders was 14.7% and 23.3% respectively.

5.2 Effect of CFRP width-to-spacing ratio

In order to investigate the effect of CFRP width-to-spacing ratio ($w_{\text{cfrp}}/s_{\text{cfrp}}$), a FE model nominally identical to those validated in Section 4, but with the EB CFRP reinforcement attached to the full span, was developed. Hence, three CFRP width-to-spacing ratios were considered, namely 0.3 (i.e. 76 mm / 254 mm), 0.6 (i.e. 76 mm / 127 mm), and 1.0 (i.e. continuous CFRP reinforcement).

As can be seen in Fig. 9, the predicted results suggest that both the shear force capacity and the contribution of the EB CFRP reinforcement increase linearly with the increase in CFRP width-to-spacing ratio. The predicted CFRP contribution increased from 22.9 KN (17.6%) to 44.3 KN (34.2%) when the CFRP width-to-spacing ratio was increased from 0.3 to 1.0. The linear variation between the CFRP contribution and the CFRP width-to-spacing ratio is adopted by existing design guidelines (ACI 440.2R-08 2008; Concrete Society TR55 2012). It is based on the truss analogy which models the EB CFRP reinforcement as external shear links that contribute to the shear resistance by controlling and limiting the progress of inclined cracks.

5.3 Effect of CFRP thickness

The effect of CFRP thickness was studied by modelling PC girders nominally identical to the strengthened models validated in Section 4. Three CFRP thickness values were considered for each series, namely 1.25 mm (i.e. similar to the experimental value), 2.50 mm, and 3.75 mm.

Figs. 10a and 10b show the variation of predicted shear force capacity and predicted CFRP contribution with CFRP thickness respectively. Similar to the effect of CFRP width-to-spacing ratio, the increase in CFRP thickness enhanced the predicted CFRP contribution and consequently the predicted shear force capacity. The predicted CFRP contributions of IB-10 and IB-05 girders increased from 22.9 (17.6%) and 32.5 KN (25.1%) respectively to 32.5 KN (25.1%) and 50.2 KN (38.8%) respectively when the CFRP thickness was increased from 1.25 mm to 3.75 mm. This may be attributed to the fact that thicker CFRP reinforcement have higher axial rigidity and therefore provide higher resistance to crack propagation.

5.4 Effect of effective girder depth

Effective depth is a major factor affecting both the shear force capacity and behaviour of concrete beams/girders. However, its influence on the shear force capacity of CFRP-strengthened PC girders has not been fully investigated. In concrete members without

internal shear reinforcement, the increase in effective depth is associated with a strong size effect (Bažant and Cao 1986; Tan et al. 2005), which may be defined as the reduction in shear stress at failure of deeper sections attributable to wider shear cracks (Dirar et al. 2013a). The girder width has no or very limited influence on the shear behaviour (Kani 1967) and therefore was not considered in this study.

In addition to the FE models developed for Control, IB-10, and IB-05 girders, which had an effective depth (d) of 457 mm, additional FE models with effective depths of 343 mm (i.e. $0.75d$) and 686 mm (i.e. $1.5d$) were developed for each series in order to investigate the influence of effective girder depth. Other parameters; such as a/d , prestressing tendons ratio, and longitudinal steel ratio; were kept constant.

Fig. 11a shows that the predicted shear stress at failure drops significantly with the increase in effective girder depth, suggesting a strong size effect in both unstrengthened and CFRP-strengthened PC girders without internal shear reinforcement. The shear stress at failure for the control, IB-10, and IB-05 series decreased by 24.7%, 26.1%, and 23.3% respectively when the effective depth was increased from 343 mm to 686 mm. As explained above, this reduction may be attributed to wider shear cracks in deeper sections.

The influence of effective girder depth on the percentage CFRP contribution is presented in Fig. 11b. It can be seen that for effective depths lower than 457 mm, the percentage CFRP contribution increases with the increase in effective beam depth. Size effect is likely to be negligible within such relatively low effective depth values. Hence the increase in effective girder depth leads to a corresponding increase in the CFRP effective bond length which, in turn, enhances the CFRP contribution. On the other hand, for effective depths higher than 457 mm, the percentage CFRP contribution decreases with the increase in effective beam depth. This reduction may be related to size effect. Further experimental testing is required to confirm the predicted results.

5.5 Effect of shear span to effective depth ratio

The shear span to effective depth (a/d) ratio is one of the significant factors that influence the shear behaviour and failure mode. A concrete member with a/d ratio less than 2.5 resists shear forces by arch-action whereas a member with a/d ratio greater than 2.5 resists shear forces by beam-action. Recent research work (Sayed et al. 2013) on FRP-strengthened reinforced concrete (RC) beams has revealed that the FRP contribution depends strongly on a/d ratio. Research investigations on the effect of a/d ratio on CFRP-strengthened PC girders are scarce.

FE models nominally identical to those validated in Section 4, but with varying shear spans, were developed. Shear span to effective depth ratios in the range of 2.5 - 5.5 were considered in this study. Fig. 12a shows the influence of a/d ratio on the predicted shear force capacity. The results, which are in accordance with the findings of Kani et al. (1979) for RC beams, reveal that the higher the a/d ratio, the lower the shear force capacity. This reduction may be related to the shift from arch-action, which provides higher resistance, to beam-action.

Fig. 12b presents the influence of a/d on the predicted CFRP contribution. The general trend that can be observed in Fig. 12b is that the predicted CFRP contribution decreased with the increase in a/d ratio. The CFRP contributions of series IB-05 and IB-10 decreased by 69% and 71.5% respectively when a/d ratio was increased from 2.5 to 5.5. This result is important because current design guidelines (ACI 440.2R-08 2008; Concrete Society TR55 2012) do not consider the effect of a/d on the CFRP contribution.

5.6 Effect of prestress

In order to investigate the effect of axial prestress, FE models nominally identical to those validated in Section 4, but with different levels of prestress in the tendons, were developed. Three levels of prestress in the tendons were considered, namely 830 MPa, 1075 MPa, and 1328 MPa. These prestress levels represented 50%, 65%, and 80% of the tendon yield strength respectively.

Except for the FE model for IB-10 with a prestress level of 1328 MPa, Fig. 13a shows that the predicted shear force capacity is marginally enhanced by the increase in axial prestress. The percentage increase in the predicted shear force capacity of the modelled girders varied from 3.97% to 6.75% when the tendon prestress level was increased from 830 MPa to 1328 MPa. The axial prestress reduces crack widths and consequently enhances the concrete contribution to the shear force capacity.

Fig. 13b presents the variation of predicted CFRP contribution with prestress level. Except for the FE model for IB-10 with a prestress level of 1328 MPa, the change in prestress level did not have a significant effect on the predicted CFRP contribution. The marginal increase in the predicted shear force capacity of the strengthened girders (see Fig. 13a) is therefore caused by the increase in predicted concrete contribution as explained above.

5.7 Effect of tendon profile

For simply supported beams, it is well known that when a parabolic or harped tendon profile is used, a resultant upward force, which may enhance the shear force capacity, acts on the concrete section. Therefore, the effect of tendon profile was investigated by developing FE models nominally identical to those validated in Section 4 but with a double-harped tendon profile. At girder ends, the tendons were positioned at the concrete centroid. They descended linearly to the level of the straight tendon at loading points (see Fig. 14).

The predicted shear force capacities of the control, IB-10, and IB-05 girders with a double-harped tendon profile were 154.9 KN, 169.5 KN, and 180.0 KN respectively. This represents an increase of 19.6%, 11.2% and 11.1% respectively over the predicted shear strength of the corresponding girders with a straight tendons profile.

The predicted CFRP contributions of IB-10 and IB-05 girders with a double-harped tendon profile were 14.6 KN and 25.1 KN respectively whereas the predicted CFRP contributions for the corresponding girders with a straight tendon profile were 22.9 KN and 32.5 KN respectively. This result indicates that, for the girders with a double-harped tendon profile,

the concrete contribution increased whereas the CFRP contribution decreased. Further research is required to better understand the interaction between tendon profile and the CFRP contribution to the shear force capacity.

5.8 Effect of pre-cracking

EB CFRP reinforcement may be used to strengthen cracked PC members. Hence, it is important to investigate the effect of pre-cracking on the shear force capacity of CFRP-strengthened PC girders. To accomplish this, six FE models nominally identical to those for IB-05 and IB-10, were developed. The nonlinear analysis of these models included three calculation phases. In Phase I, the unstrengthened FE models, with the elements representing the EB CFRP reinforcement and the FRP-to-concrete interface set as inactive, were prestressed. Phase II included loading the unstrengthened FE models to 75%, 85% or 95% of their unstrengthened shear force capacity. Phase III included activating the elements representing the EB CFRP reinforcement and the FRP-to-concrete interface, and then loading the FE models up to failure.

Fig. 15 presents the variation of predicted shear force capacity with normalised pre-crack load (pre-cracking level). It can be seen that, up to a pre-cracking level of 85%, there was no significant effect on the predicted shear strength. Comparable results (Dirar et al. 2012) were reported for CFRP-strengthened RC beams where it was found that a pre-cracking level of 70% had insignificant effect on the shear force capacity. At a pre-cracking level of 95%, the EB CFRP strips enhanced the shear force capacity of IB-10 and IB-05 girders by 5.5 KN (4.2%) and 3.98 KN (3.1%) respectively. Failure was governed by excessive opening of the existing diagonal cracks. The results imply that EB CFRP reinforcement can be effectively used to retrofit cracked PC girders.

5.9 Effect of CFRP-to-Concrete bond-slip model

The CFRP-to-concrete bond-slip model plays an important role in FE modelling of concrete structures strengthened with EB CFRP reinforcement. In addition to the bond-slip model

adopted in this study (Sato and Vecchio 2003), the simplified bond-slip model proposed by Lu et al. (2005) was considered. The latter model assumes that the bond stress varies nonlinearly with slip (for more details see Lu et al. 2005). For approximately equal values of peak bond stress and interfacial fracture energy, the predictions of the two bond-slip models were practically similar suggesting that the shape of the bond-slip model had no influence on the overall behaviour. Similar findings were reported by Niu and Wu (2006).

6 Conclusions

This paper presents a three-dimensional nonlinear FE model for PC girders strengthened in shear with EB CFRP strips. The FE model was validated using experimental results from the published literature. An extensive parametric study was carried out to investigate the effect of the concrete compressive strength, CFRP width-to-spacing ratio, CFRP thickness, girder effective depth, shear span to effective depth ratio, level of prestress, tendon profile, pre-cracking and CFRP-to-concrete interface model on the predicted the shear force capacity.

Based on the obtained numerical results, the following conclusions were drawn. Further experimental testing is recommended to confirm the FE-predicted results and increase the database of PC girders strengthened in shear with EB CFRP reinforcement.

1. The concrete compressive strength had a significant influence on both the concrete and CFRP contributions to the predicted shear force capacity. The percentage increase in predicted shear force capacity ranged from 61.3% to 65.1% when the concrete compressive strength was increased from 30 to 70 MPa.
2. The predicted CFRP contribution increased from 22.9 KN (17.6%) to 44.3 KN (34.2%) when the CFRP width-to-spacing ratio was increased from 0.3 to 1.0.
3. The increase in the CFRP thickness enhanced the predicted CFRP contribution and consequently the predicted shear force capacity. The percentage increase in CFRP

contribution to the shear force capacity ranged from 17.6% to 38.8% when the CFRP thickness was increased from 1.25 mm to 3.75 mm.

4. A strong size effect was predicted for both the unstrengthened and CFRP-strengthened PC girders without internal shear reinforcement. The percentage reduction in predicted shear stress at failure ranged from 23.3% to 26.1% when the effective depth was increased from 343 mm to 686 mm.
5. The predicted CFRP contributions of the strengthened beams decreased by 69% to 71.5% when the shear span to effective depth ratio was increased from 2.5 to 5.5.
6. The level of prestress in the tendons significantly influenced neither the predicted CFRP contribution nor the predicted shear force capacity.
7. The change in tendon profile from a straight to double-harped shape increased the predicted total shear force capacity but had a detrimental effect on the predicted CFRP contribution to the shear force capacity.
8. Pre-cracking loads of up to 85% of the unstrengthened shear force capacity did not have a significant effect on the predicted strengthened capacity. At higher pre-cracking load levels, the predicted CFRP contribution was insignificant.
9. For approximately equal values of peak bond stress and interfacial fracture energy, the shape of the CFRP-to-concrete bond-slip model had no influence on the overall behaviour of the modelled girders.

Acknowledgements

The first author gratefully acknowledges the financial support of KRG.

References

American Concrete Institute ACI 440R-07 (2007), Report on fiber-reinforced polymer (FRP) reinforcement for concrete structures. Farmington Hills, Michigan, USA, 100 pp.

American Concrete Institute ACI 440.2R-08 (2008), Guide for the design and construction of externally bonded FRP systems for strengthening concrete structures. Farmington Hills, Michigan, USA, 76 pp.

Bažant, Z.P.; Cao, Z. (1986), Size effect of shear failure in prestressed concrete beams. ACI Journal, Vol. 83, No. 2, pp. 260-268.

Bažant, Z.P.; Oh, B.H. (1983), Crack band theory for fracture of concrete. Materials and Structures, Vol. 16, No. 3, pp. 155-177.

CEB-FIP Model Code 1990 (1993), Design code. Thomas Telford, London.

Concrete Society TR 55 (2012), Design guidance for strengthening concrete structures using fibre composite materials. Crowthorne, UK, 187 pp.

DIANA. (2012), User's Manual, Version 9.4.4., TNO DIANA BV, Delft, The Netherlands.

Dirar, S.; Lees, J.; Morley, C. (2012), Precracked reinforced concrete T-beams repaired in shear with bonded carbon fiber-reinforced polymer sheets. ACI Structural Journal, Vol. 109, No. 2, pp. 215-224.

Dirar, S.; Lees, J.M.; Morley, C.T. (2013a), Precracked reinforced concrete T-beams repaired in shear with prestressed carbon fiber-reinforced polymer straps. ACI Structural Journal, Vol. 110, No. 5, pp. 855-866.

Dirar, S.; Lees, J.M.; Morley, C. (2013b), Phased nonlinear finite-element analysis of precracked RC T-beams repaired in shear with CFRP sheets. ASCE Journal of Composites for Construction, Vol. 17, No. 4, pp. 476-487.

Hee, S.C.; Jefferson, A.D. (2008), A new model for simulating cracks in cementitious composites. Proceedings of the ICE – Engineering and Computational Mechanics, Vol. 161, No. 1, pp. 3-16.

- Kang, T.H.K.; Ary, M.I. (2012), Shear-strengthening of reinforced & prestressed concrete beams using FRP: Part II – experimental investigation. *International Journal of Concrete Structures and Materials*, Vol. 6, No. 1, pp. 49-57.
- Kani, G.N.J (1967), How safe are our large reinforced concrete beams?. *ACI Journal*, Vol. 64, No. 3, pp. 128-141.
- Kani, G.; Huggins, M.W.; Wittkopp, R.R. (1979), Kani on shear in reinforced concrete. Department of Civil Engineering, University of Toronto, Canada, 225 pp.
- Lu, X.Z.; Teng, J.G.; Ye, L.P.; Jiang, J.J. (2005), Bond-slip models for FRP sheets/plates bonded to concrete. *Engineering Structures*, Vol. 27, No. 6, pp. 920-937.
- Middleton, C.R. (1997), Concrete bridge assessment: An alternative approach. *The Structural Engineer*, Vol. 75, No. 23/24, pp. 403-409.
- Murphy, M.; Belarbi, A.; Bae, S-W. (2012), Behavior of prestressed concrete I-girders strengthened in shear with externally bonded fiber-reinforced-polymer sheets. *PCI Journal*, Vol. 57, No. 3, pp. 63-82.
- Nanni, A.; Ludovico, M.D.; Parretti, R. (2004), Shear strengthening of a PC bridge girder with NSM CFRP rectangular bars. *Advances in Structural Engineering*, Vol. 7, No. 4, pp. 97-109.
- Niu, H.; Wu, Z. (2006), Effects of FRP-concrete interface bond properties on the performance of RC beams strengthened in flexure with externally bonded FRP sheets. *ASCE Journal of Materials in Civil Engineering*, Vol. 18, No. 5, pp. 723-731.
- Petty, D.A.; Barr, P.J.; Osborn, G.P.; Halling, M.W.; Brackus, T.R. (2011), Carbon fiber shear retrofit of forty-two-year-old AASHTO I-shaped girders. *ASCE Journal of Composites for Construction*, Vol. 15, No. 5, pp. 773-781.

- Sagaseta, J.; Vollum, R.L. (2009), Non-linear finite element analysis of shear critical high strength concrete beams. *Architecture Civil Engineering Environment – ACEE*, Vol. 2, No. 4, pp. 95-106.
- Sato, Y.; Vecchio, F.J. (2003), Tension stiffening and crack formation in reinforced concrete members with fiber-reinforced polymer sheets. *ASCE Journal of Structural Engineering*, Vol. 129, No. 6, pp. 717-724.
- Sayed, A.; Wang, X.; Wu, Z. (2013), Modeling of shear capacity of RC beams strengthened with FRP sheets based on FE simulation. *Journal of Composites for Construction*, Vol. 17, No. 5, pp. 687-701.
- Tan, K.H.; Cheng, G.H.; Cheong, H.K. (2005), Size effect in shear strength of large beams behaviour and finite element modelling. *Magazine of Concrete Research*, Vol. 57, No. 8, pp. 497-509.
- Thorenfeldt, E.; Tomaszewicz, A.; Jensen, J.J. (1987), Mechanical properties of high-strength concrete and applications in design. *Proc. Symp. Utilization of High-Strength Concrete*, Tapir, Trondheim, Norway, pp. 149-159.
- Valerio, P.; Ibell, T.J.; Darby, A.P. (2009), Deep embedment of FRP for concrete shear strengthening. *Proceedings of the Institution of Civil Engineers - Structures and Buildings*, Vol. 162, No. 5, pp. 311-321.
- Vecchio, F.J.; Collins, M.P. (1993), Compression response of cracked reinforced concrete. *ASCE Journal of Structural Engineering*, Vol. 119, No. 12, pp. 3590-3610.
- You, Y.M.; Ayoub, A.; Belarbi, A. (2011), Three-dimensional nonlinear finite-element analysis of prestressed concrete beams strengthened in shear with FRP composites. *ASCE Journal of Composites for Construction*, Vol. 15, No. 6, pp. 896-907.

LIST OF TABLES

Table 1 Material properties

Table 2 Experimental and FE results

Table 1 Material properties

Material	Elastic modulus (MPa)	Cylinder compressive strength (MPa)	Modulus of rupture (MPa)	Ultimate strain mm/mm	Yield strength (MPa)	Ultimate strength (MPa)
Concrete	39314	59.0	4.9	-	-	-
Ø10 mm bar	198927	-	-	-	439.2	699.0
Ø12 mm bar	186648	-	-	-	414.4	711.5
Ø20 mm bar	204547	-	-	-	476.4	766.0
Ø25 mm bar	192922	-	-	-	433.0	752.2
Ø12.5 mm tendon	200548	-	-	-	1656.8	1811.2
CFRP strips	6585	-	-	0.015	-	98.7

Table 2 Experimental and FE results

Beam	V Exp. (KN)	V FE (KN)	$\frac{V \text{ Exp.}}{V \text{ FE}}$	Δ Exp. (mm)	Δ FE (mm)	$\frac{\Delta \text{ Exp.}}{\Delta \text{ FE}}$
Control	117.4	129.5	0.91	12.58	11.33	1.11
IB-05	161.9	162.0	1.00	16.13	14.38	1.12
IB-10	119.2	149.7	0.80	12.34	13.18	0.94

LIST OF FIGURES

Fig. 1 Unstrengthened cross-section of the tested girders (Kang and Ary 2012)

Fig. 2 Details of tested PC girders: (a) control specimen, (b) IB-05, and (c) IB-10 (Kang and Ary 2012)

Fig. 3 Finite element model

Fig. 4 Stress-strain curve for the prestressing tendons (Kang and Ary 2012)

Fig. 5 CFRP-to-concrete bond-slip model (Sato and Vecchio 2003)

Fig. 6 Shear force versus mid-span deflection curves: (a) control specimen, (b) IB-05, and (c) IB-10 (modelled using concrete compressive strengths of 45 MPa and 59 MPa)

Fig. 7 Experimental (Kang and Ary 2012) and numerical failure modes: (a) control specimen, (b) IB-05, and (c) IB-10

Fig. 8 Effect of concrete compressive strength on (a) the predicted shear force capacity and (b) the predicted shear force gain due to the EB CFRP reinforcement

Fig. 9 Effect of CFRP width-to-spacing ratio on (a) the predicted shear force capacity and (b) the predicted shear force gain due to the EB CFRP reinforcement

Fig. 10 Effect of CFRP thickness on (a) the predicted shear force capacity and (b) the predicted shear force gain due to the EB CFRP reinforcement

Fig. 11 Effect of effective girder depth on (a) the predicted shear stress at failure and (b) the predicted percentage shear force gain due to the EB CFRP reinforcement

Fig. 12 Effect of shear span to effective beam depth on (a) the predicted shear force capacity and (b) the predicted shear force gain due to the EB CFRP reinforcement

Fig. 13 Effect of prestress on (a) the predicted shear force capacity and (b) the predicted shear force gain due to the EB CFRP reinforcement

Fig. 14 Double-harped tendon profile

Fig. 15 Effect of pre-cracking level on the predicted shear force capacity

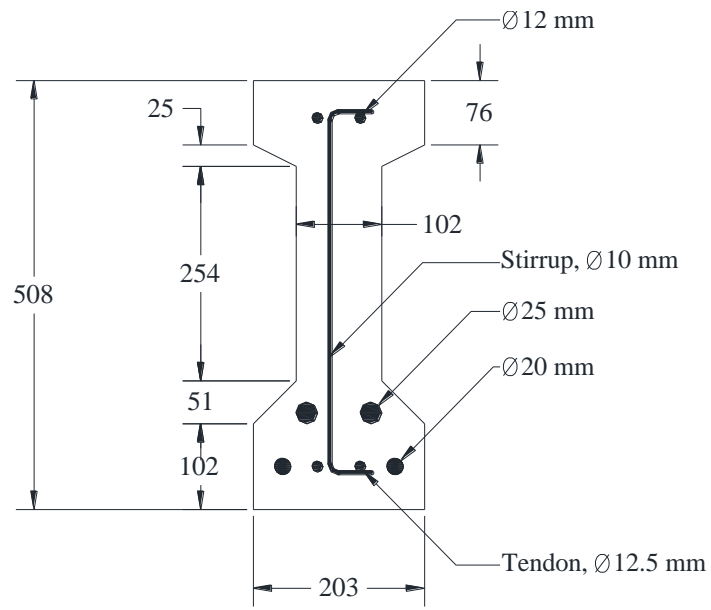


Fig. 1 Unstrengthened cross-section of the tested girders (Kang and Ary 2012)

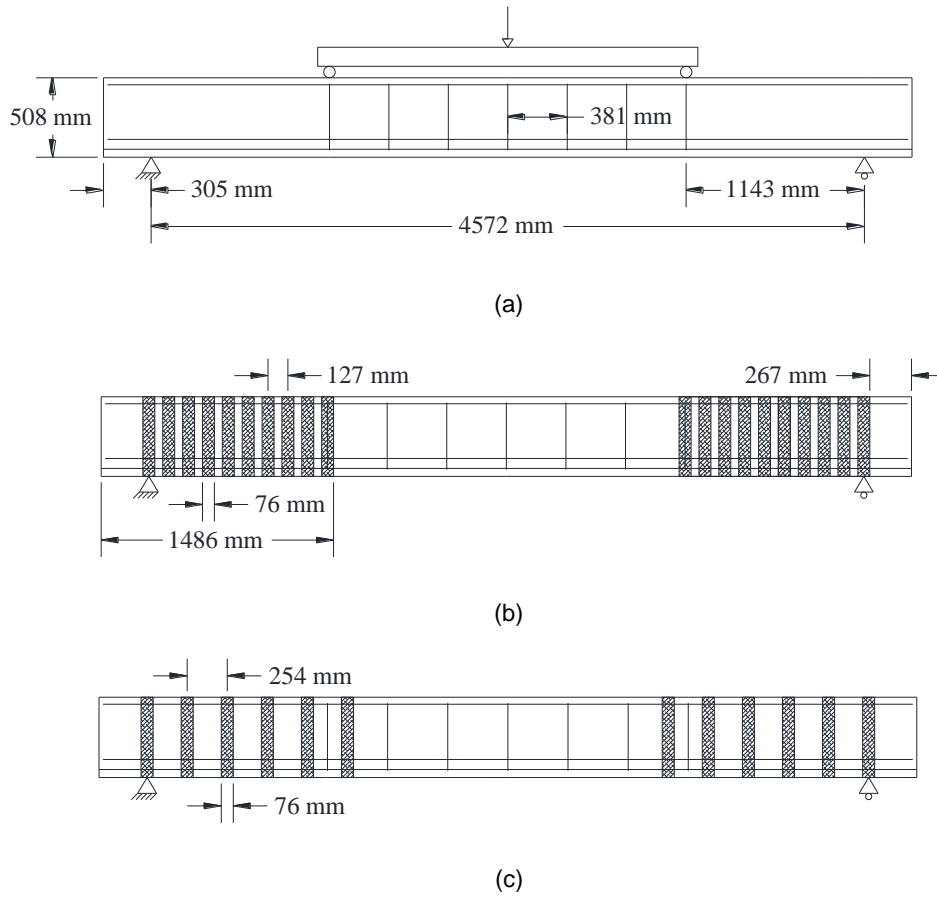


Fig. 2 Details of tested PC girders: (a) control specimen, (b) IB-05, and (c) IB-10 (Kang and Ary 2012)

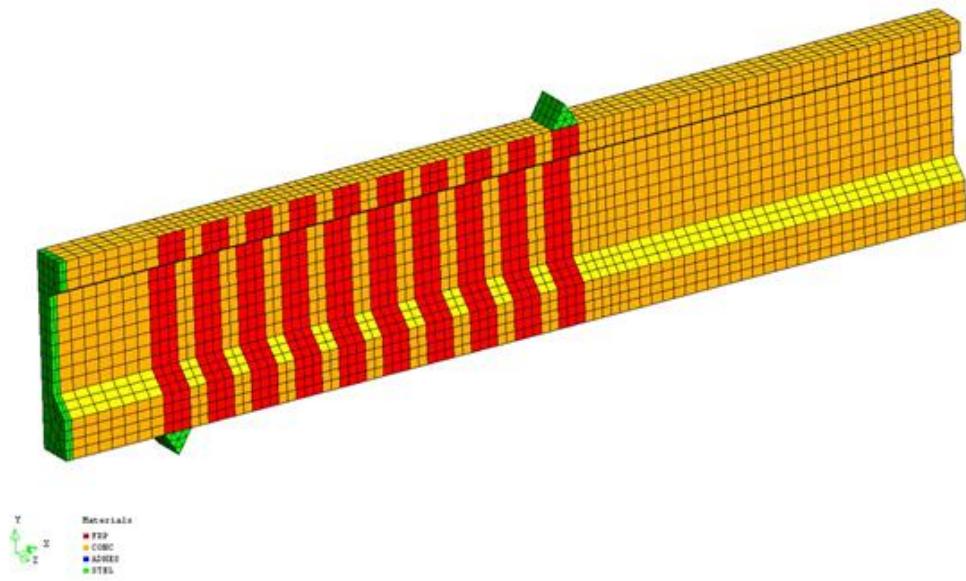


Fig.3 Finite element model

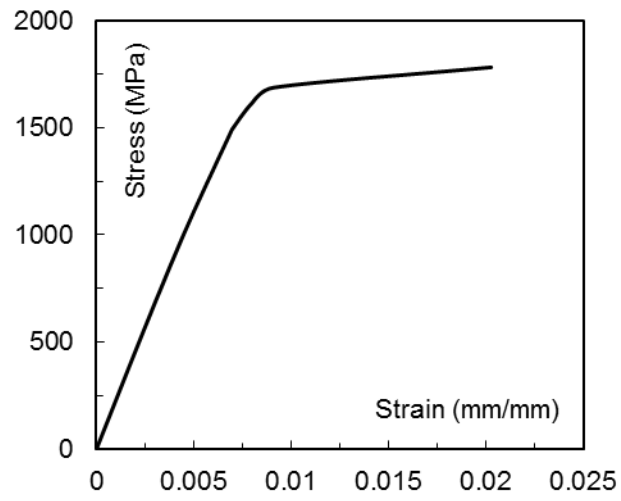


Fig. 4 Stress-strain curve for the prestressing tendons (Kang and Ary 2012)

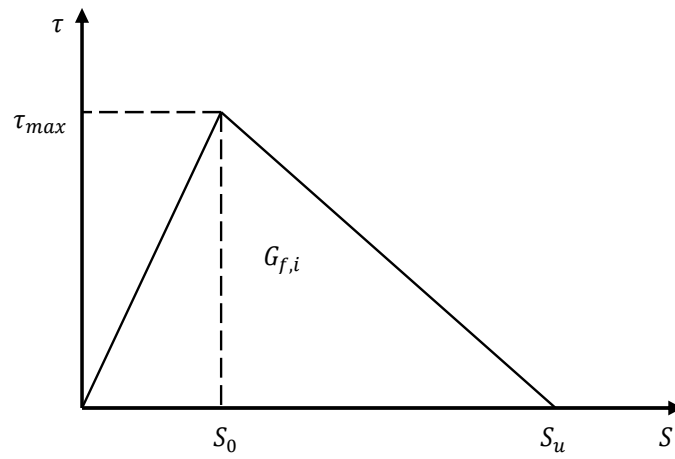
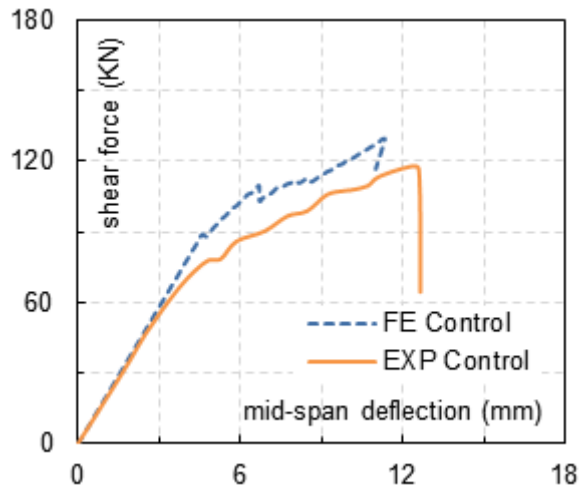
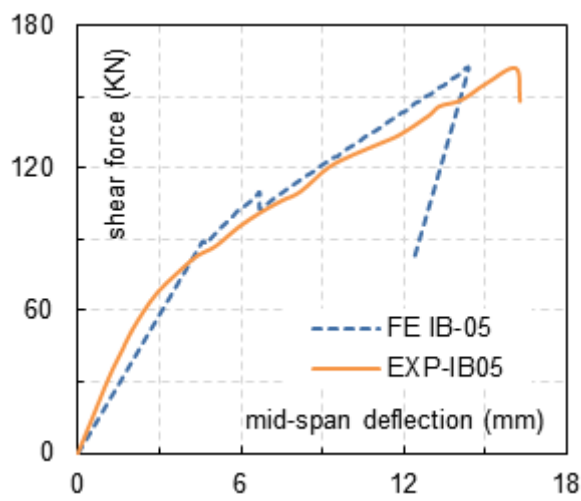


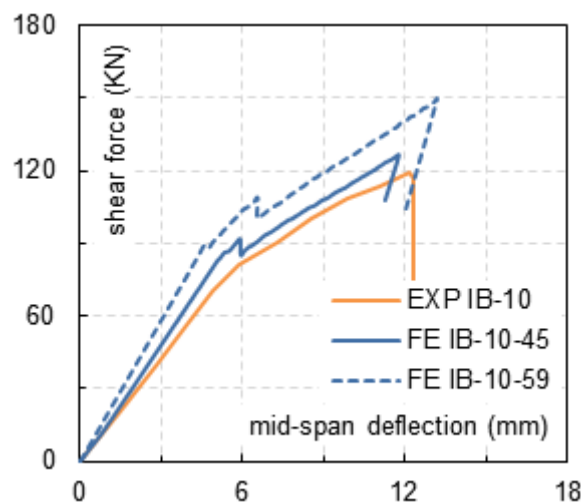
Fig. 5 CFRP-to-concrete bond-slip model (Sato and Vecchio 2003)



(a)

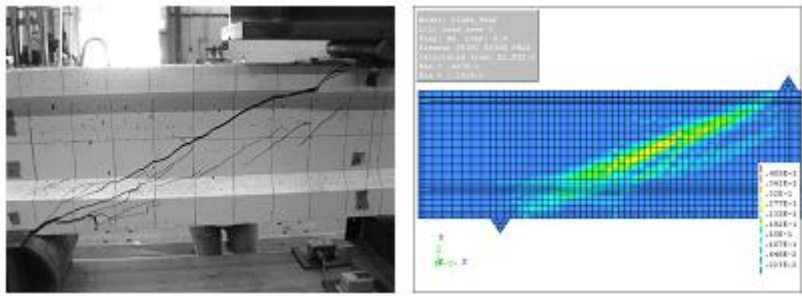


(b)

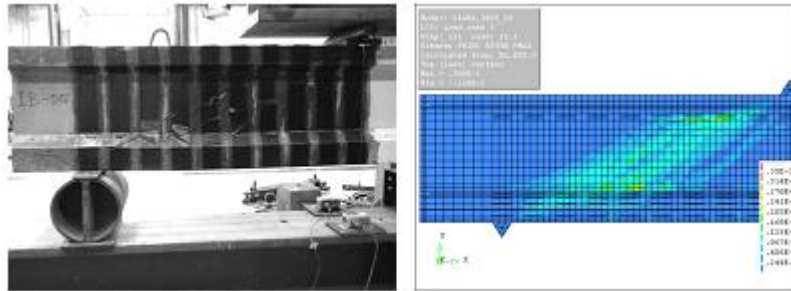


(c)

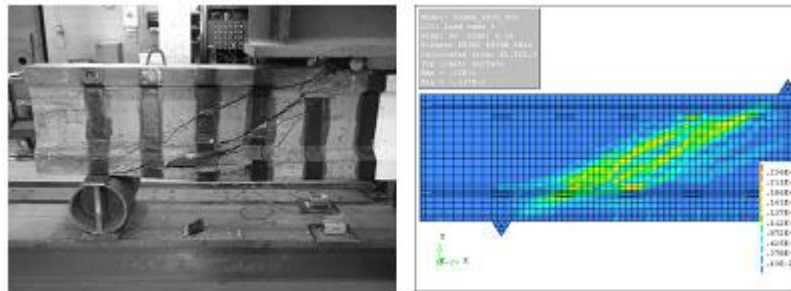
Fig. 6 Shear force versus mid-span deflection curves: (a) control specimen, (b) IB-05, and (c) IB-10 (modelled using concrete compressive strengths of 45 MPa and 59 MPa)



(a)



(b)



(c)

Fig. 7 Experimental (Kang and Ary 2012) and numerical failure modes: (a) control specimen, (b) IB-05, and (c) IB-10

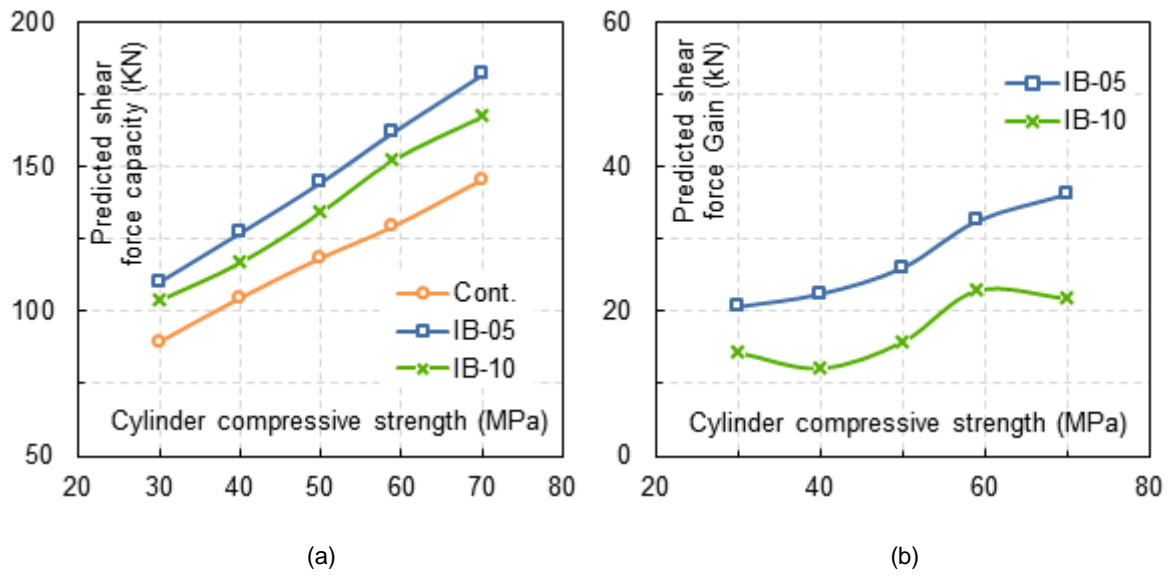


Fig. 8 Effect of concrete compressive strength on (a) the predicted shear force capacity and (b) the predicted shear force gain due to the EB CFRP reinforcement

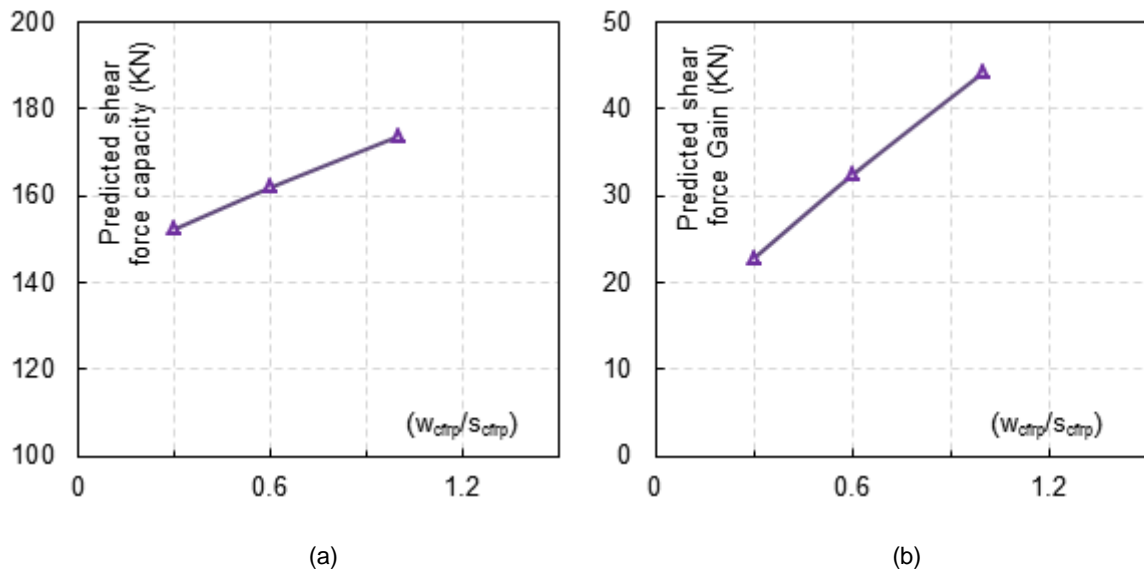


Fig. 9 Effect of CFRP width-to-spacing ratio on (a) the predicted shear force capacity and (b) the predicted shear force gain due to the EB CFRP reinforcement

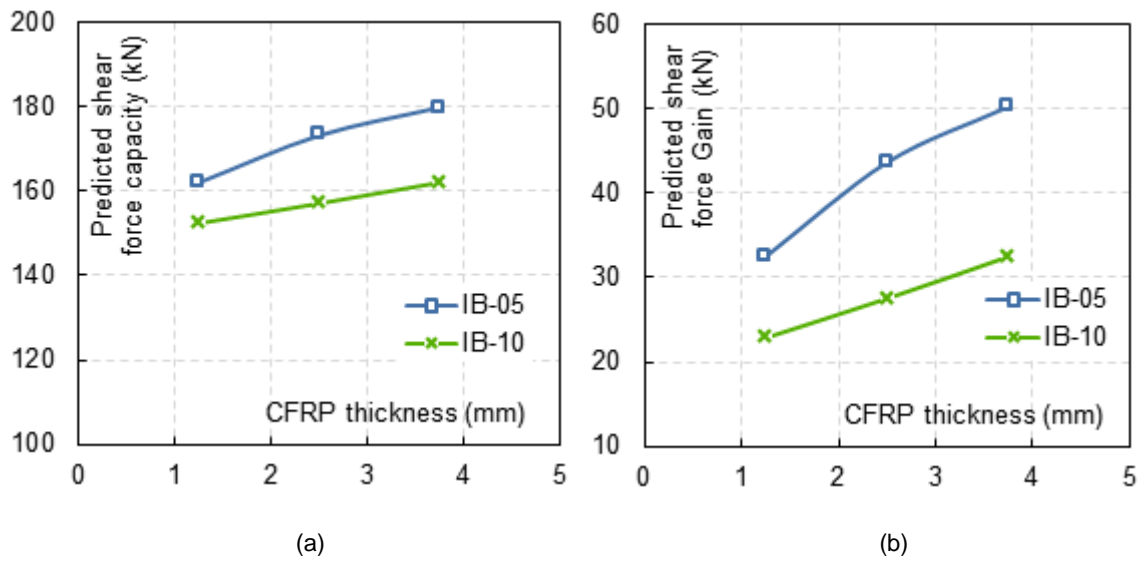


Fig. 10 Effect of CFRP thickness on (a) the predicted shear force capacity and (b) the predicted shear force gain due to the EB CFRP reinforcement

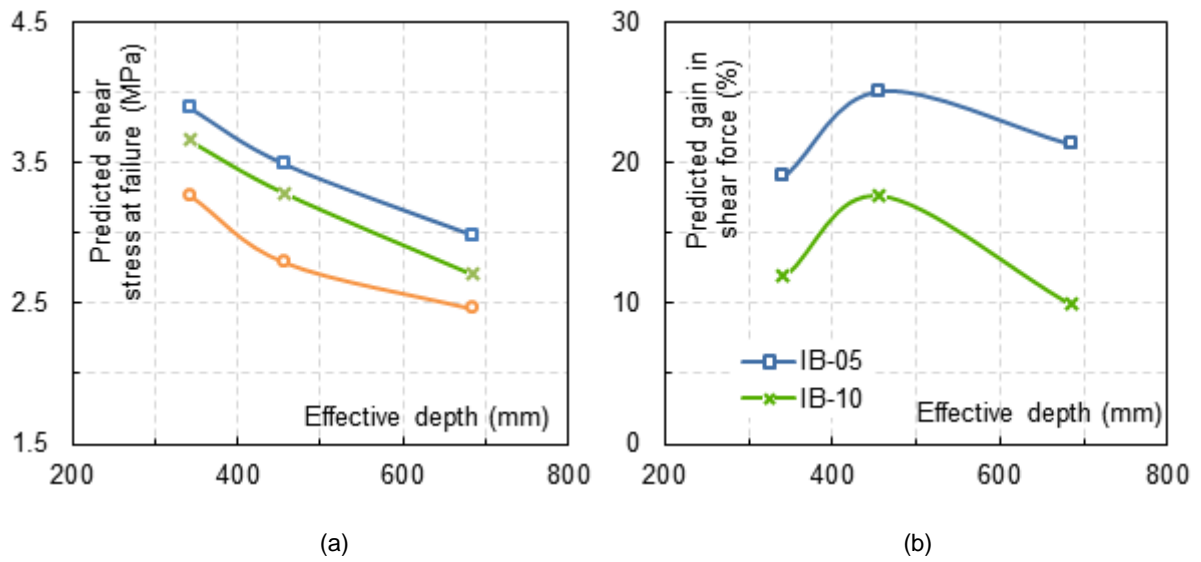


Fig. 11 Effect of effective girder depth on (a) the predicted shear stress at failure and (b) the predicted percentage shear force gain due to the EB CFRP reinforcement

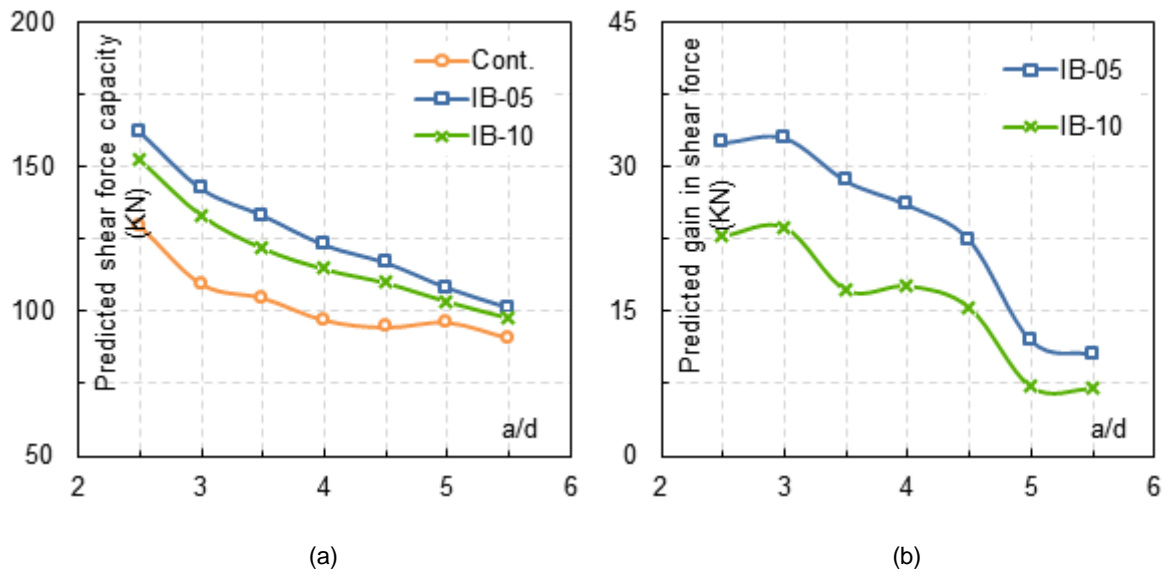


Fig. 12 Effect of shear span to effective beam depth on (a) the predicted shear force capacity and (b) the predicted shear force gain due to the EB CFRP reinforcement

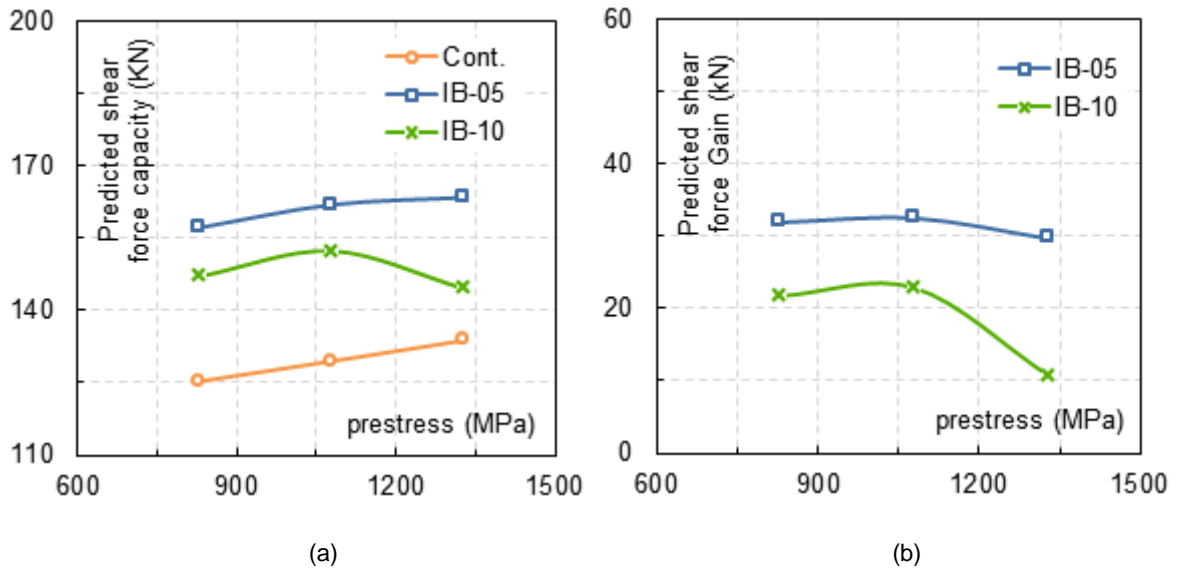


Fig. 13 Effect of prestress on (a) the predicted shear force capacity and (b) the predicted shear force gain due to the EB CFRP reinforcement

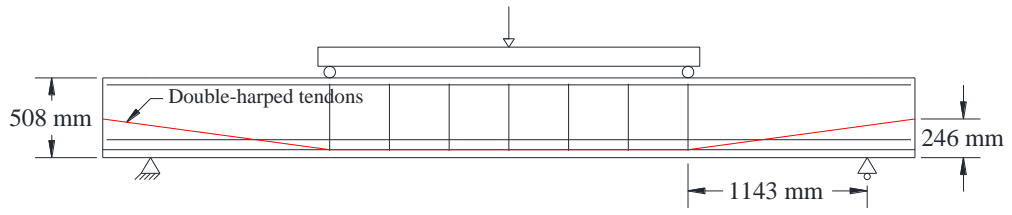


Fig. 14 Double-harped tendon profile

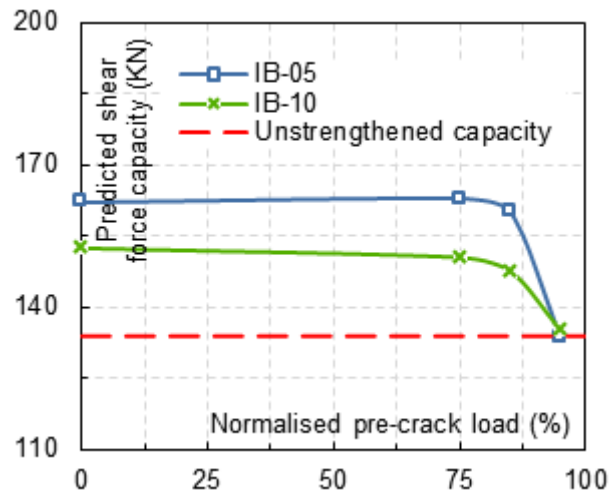


Fig. 15 Effect of pre-cracking level on the predicted shear force capacity